Mapped Interpolation Scheme for Single-Point Energy Corrections in Reaction Rate Calculations and a Critical Evaluation of Dual-Level Reaction Path Dynamics Methods

ARTICLE *in* THE JOURNAL OF PHYSICAL CHEMISTRY A · FEBRUARY 1999

Impact Factor: 2.69 · DOI: 10.1021/jp9842493

3 AUTHORS:

Yao-Yuan Chuang
National University of Kaohsiung
42 PUBLICATIONS **1,318** CITATIONS
SEE PROFILE

Jose C Corchado
Universidad de Extremadura
118 PUBLICATIONS **3,273** CITATIONS
SEE PROFILE

Donald Truhlar
University of Minnesota Twin Cities
1,342 PUBLICATIONS **79,615** CITATIONS
SEE PROFILE

1140 *J. Phys. Chem. A* **1999**, *103*, 1140−1149 (Submitted as a Reprint)

Mapped Interpolation Scheme for Single-Point Energy Corrections in Reaction Rate Calculations and a Critical Evaluation of Dual-Level Reaction Path Dynamics Methods

Yao-Yuan Chuang,[†] José C. Corchado,[‡] and Donald G. Truhlar*,[†]

Department of Chemistry and Supercomputer Institute, University of Minnesota, Minneapolis, Minnesota 55455-0431, and Departamento de Química Física, Universidad de Extremadura, Badajoz 06071, Spain

Received: October 28, 1998; In Final Form: December 23, 1998

Three procedures for incorporating higher level electronic structure data into reaction path dynamics calculations are tested. In one procedure, variational transition state theory with interpolated single-point energies, which is denoted VTST-ISPE, a few extra energies calculated with a higher level theory along the lower level reaction path are used to correct the classical energetic profile of the reaction. In the second procedure, denoted variational transition state theory with interpolated optimized corrections (VTST-IOC), which we introduced earlier, higher level corrections to energies, frequencies, and moments of inertia are based on stationary-point geometries reoptimized at a higher level than the reaction path was calculated. The third procedure, called interpolated optimized energies (IOE), is like IOC except it omits the frequency correction. Three hydrogen-transfer reactions, $CH_3 + H'H \rightarrow CH_3H' + H$ (R1), $OH + H'H \rightarrow HOH' + H$ (R2), and $OH + H'CH_3 \rightarrow HOH' + CH_3$ (R3), are used to test and validate the procedures by comparing their predictions to the reaction rate evaluated with a full variational transition state theory calculation including multidimensional tunneling (VTST/MT) at the higher level. We present a very efficient scheme for carrying out VTST-ISPE calculations, which are popular due to their lower computational cost. We also show, on the basis of calculations of the reactions R1−R3 with eight pairs of higher and lower levels, that VTST-IOC with higher level data only at stationary points is a more reliable dual-level procedure than VTST-ISPE with higher level energies all along the reaction path. Although the frequencies along the reaction path are not corrected in the IOE scheme, the results are still better than those from VTST-ISPE; this indicates the importance of optimizing the geometry at the highest possible level.

1. Introduction

Variational transition state theory (VTST) with multidimensional tunneling (MT) contributions, which we abbreviate as either VTST/MT or as semiclassical VTST (SC-VTST), has been shown to provide a practical yet accurate method for calculating chemical reaction rate constants for gas-phase[1,2] and condensed-phase[2,3] processes. Thus, there is considerable interest in developing efficient ways to carry out such calculations, especially in the context of direct dynamics,[2,4−9] an approach in which rate constants are evaluated directly from electronic structure calculations without the intermediacy of an explicit potential energy function.

Direct VTST/MT dynamics calculations require electronic structure information over an entire reaction path[3−14] and in a corner-cutting reaction swath.[6,8−11,15] In recent work,[10,11] we have shown that dual-level direct dynamics calculations can provide a powerful way to combine such information computed reasonably cost-effective lower level of electronic structure theory with selected results computed with more expensive (and presumably more reliable) electronic structure methods. We use the label VTST-IC, which denotes variational transition state theory with interpolated corrections, to refer to carrying out a VTST calculation at a lower level and then correcting the reaction path data (and possibly the reaction swath data) obtained at that level by using more limited data obtained at a higher level. One systematic version[10,11] of this approach, which we will now call VTST-IOC, where the suffix denotes interpolated optimized corrections, involves high-level geometry *optimization* at reactants, saddle point, and products. An alternative VTST-IC approach has also been used by several groups;[5,16−18] in this approach, one first calculates the reaction path at the lower level (which is also the first step in the VTST-IOC method[10,11]) but then corrects the energy along the reaction path *without* reoptimizing any geometries. (The motivation for this simplification is that geometry optimization is very expensive, and for high enough higher levels, it is prohibitively expensive). In keeping with a widely accepted language used in quantum chemistry, such calculations are called "single-point energies". Thus, to distinguish the two VTST-IC approaches, we called the former VTST-IOC to denote interpolated optimized corrections and the latter VTST-ISPE to denote interpolated single-point energies. We will also test a simpler version of the VTST-IOC method, called VTST with interpolated optimized energies (VTST-IOE), in which the higher level frequency calculation is omitted.

For properties of stable species, a single-point energy calculated using level X at a geometry optimized with level Y is denoted X//Y.[19] For reaction path calculations, improving the system properties (energies, moment of inertia, and/or frequencies) by using calculations carried out with level X to correct a set of reaction path data calculated at level Y is called X//Y if

[†] University of Minnesota.
[‡] Universidad de Extremadura.

10.1021/jp9842493 CCC: $18.00
Published on Web 02/04/1999

no geometry reoptimization is performed. If, however, stationary-point geometries are reoptimized at level X, it is called X/// Y, and if the geometry is reoptimized at level X′ (intermediate between X and Y), it is called X//X′///Y. In this language, the question addressed here is to compare the X///Y and X//Y approaches to rate constant calculations. Because geometry optimization is computationally demanding, X//Y is typically less expensive than X///Y, even when many single-point energies are calculated. Since corrections are made all along the path, can the method be not only less expensive but also more accurate?

A systematic VTST-IOC algorithm was presented previously.[10,11] In section 2, we present a systematic VTST-ISPE algorithm. In section 3, we present a series of comparisons of full rate constant calculations in which we directly compare calculations at levels X, X///Y, and X//Y. These results show that a critical issue is how severely X//Y calculations along a reaction path overestimate the saddle point height $V^{\ddagger}$ calculated with geometry optimization at level X. We also present additional calculations relevant to the latter question and especially designed to see (1) if the conclusions are changed as the qualities of the X and Y levels are improved and (2) whether density functional theory[20] (DFT) or the hybrid Hartree–Fock–DFT method[21,22] is particularly useful for level Y. Section 4 summarizes the major conclusions.

2. Theory

2.1. VTST/MT. We consider four levels of dynamics calculations: TST (conventional transition state theory);[23] CVT (canonical variational theory);[24] CVT/ZCT (CVT with zero-curvature tunneling);[25] CVT/SCT (CVT with small-curvature tunneling).[26] In all four cases, vibrations are treated with the quantum mechanical harmonic oscillator approximation in curvilinear coordinates[13c,27] and rotational partition functions are evaluated by classical mechanics. Motion along the reaction coordinate is treated classically in TST and CVT and semiclassically in CVT/ZCT and CVT/SCT. In CVT/ZCT and CVT/SCT, the effective potential for tunneling is the ground-state vibrationally adiabatic potential curve[25]

$$V_a^G(s) = V_{RP}(s) + \epsilon^G(s) \tag{1}$$

where s is the signed distance along the reaction path in mass-scaled (i.e., isoinertial) coordinates (with s negative on the reactant side of the saddle point and positive on the product side), $V_{RP}(s)$ is the Born–Oppenheimer potential along the reaction path (RP), and $\epsilon^G(s)$ is the local zero-point energy. We use the convention that $V_{RP}(s)$ is zero at reactants. The transmission coefficient at temperature T is[25]

$$\kappa(T) = \beta \int_0^\infty dE P^G(E) \exp(\beta\{V_a^G[s_*^{CVT}(T)] - E\}) \tag{2}$$

where

$$\beta = 1/\tilde{k}T \tag{3}$$

$\tilde{k}$ is Boltzmann's constant, E is total energy, P^G is the ground-state transmission probability in the ZCT or SCT approximation, and s_*^{CVT} is the location of the canonical variational transition state at temperature T.

A quantity that will play an important role in the development below is the representative tunneling energy at temperature T, which we call $E_{rep}(T)$. This is defined as the maximum of the integrand of eq 2 at temperature T for the most reliable available tunneling approximation, which is the SCT approximation in the present paper. The representative turning points of the reaction coordinate are then defined by the solutions s of

$$V_a^G(s) = E_{rep}(T) \tag{4}$$

The most negative solution of eq 4 is called $s_<(T)$, and the most positive solution is called $s_>(T)$.

2.2. VTST-ISPE. To calculate the reaction rates with VTST-ISPE, one first calculates a converged RP at the lower level Y. Then, a spline under tension[28] is used to interpolate the energy difference of a few single-point energies along the RP between the higher level X with the geometries obtained at level Y and the energy from lower level Y; that is, one interpolates the difference quantity

$$\Delta V_{RP}(s) = V_{RP}^{X//Y}(s) - V_{RP}^{Y}(s) \tag{5}$$

as a function of the reaction coordinate s, which is the signed distance from the level-Y saddle point along the RP. As in our previous interpolated variational transition state theory with mapping[29] (IVTST-M) method, a mapped coordinate z is used to provide a systematic interpolating procedure for both bimolecular and unimolecular reactions. For unimolecular reactions, the domain of each mapping function extends from reactants (R) to products (P); for bimolecular reactions, it extends from R or a well in the reactant valley (reactant well, RW) to P or a well in the product valley (product well, PW). To map the reaction coordinate s into the z space, the following expression is used:

$$z = \frac{2}{\pi} \arctan\left(\frac{s - s_0}{L}\right) \tag{6}$$

Information from the lower level is used to obtain the parameters s_0 and L for the mapping. First, we define

$$s_A^0 = -\sqrt{\frac{V_{RP}(s=0) - V_{RP}(s_X)}{|\omega^{\ddagger}|^2 \mu}}; \quad X = \text{R or RW} \tag{7}$$

$$s_B^0 = \sqrt{\frac{V_{RP}(s=0) - V_{RP}(s_X)}{|\omega^{\ddagger}|^2 \mu}}; \quad X = \text{P or PW} \tag{8}$$

where μ is the scaling mass,[25] and $\omega^{\ddagger}$ is the imaginary frequency of the saddle point at the lower level. Then, we define

$$s_A = -\min(|s_A^0|, 2s_B^0) \tag{9}$$

and

$$s_B = \min(2|s_A^0|, s_B^0) \tag{10}$$

Then the parameters of eq 6 are obtained from these parameters by

$$s_0 = \frac{s_A + s_B}{2} \tag{11}$$

and

$$L = \frac{|s_A| + s_B}{2} \tag{12}$$

For unimolecular reactions, the mapping is from a finite interval in s to a finite interval in z. For the bimolecular reactions, the reaction coordinate s is located between $[-\infty, \infty]$, but we may

choose to recognize a well in the reactant and/or product valley.[29] Thus, the mapping is from an infinite, semi-infinite, or finite range of s to a finite range of z. In all cases, we apply the spline fit to the differences of the Born–Oppenheimer energies within the finite range of z. We write the dual-level interpolated energy as

$$V_{RP}^{DL}(s) = V_{RP}^{LL}(s) + \text{spline}(\Delta V_{RP}(s), z) \qquad (13)$$

where DL is dual level (i.e., VTST-ISPE level, denoted X//Y) and LL is the lower level (i.e., Y).

To have a general, testable method, we must systematize not only the algorithm for interpolation, which we have just presented, but also the scheme for where to place the extra energies, which we discuss next. We will use the notation VTST-ISPE-$n(l)$, where n denotes the number of nonstationary points along the path at which single-point energies are calculated and l is a list of their positions in reduced units. The reduced unit is different on the reactant and product side of the saddle point and is called α on the reactant side and α' on the product side. We take α as $s_<(T = 300\ \text{K})$ and α' as $s_>(T = 300\ \text{K})$, where these values are evaluated by a full tunneling calculation at the lower level.

The notation is most clearly specified by an example. Consider the specification VTST-ISPE-4(±0.1, ±1.2), this means that the interpolation of eq 5 is based on single-point energies evaluated at seven points, namely reactants or a reactant well, the saddle point, products or a product well, and four nonstationary points. (Note that one always requires reactant information for a rate constant calculation so that if interpolation is based on a reactant well, one requires an eighth single-point energy at reactants.) In addition, the example specification denotes that the nonstationary points are at ±0.1, ±1.2 in reduced units, i.e., at $s = -1.2\alpha, -0.1\alpha, +0.1\alpha', +1.2\alpha'$. Note that α and α' are evaluated from the low-level SCT calculation at 300 K for all ISPE calculations, even those at the ZCT level or for temperatures above or below 300 K. The goal is to use a single set of points to carry out a set of calculations over a range of temperatures.

This interpolation procedure is general for all cases. When $n = 0$, the differences of energies at three stationary points (i.e., reactants, products, and saddle point) are used for spline fit for eq 13. We use the convention of setting the energies of the reactants to zero; therefore, the sum of the energies of the products is the energy of reaction.

2.3. VTST-IOC. For comparison, we will also report some results obtained with the VTST-IOC method. These methods have been described previously,[10,11] and our general procedure involves two options, called SECKART and DECKART, for interpolating V_{RP} and three options, called ICA, ICR, and ICL for interpolating vibrational frequencies. In this paper, we use three combinations: (i) the original SECKART-ICA method,[10] (ii) the DECKART-ICL combination recommended later,[11] and the combination we now favor on the basis of considerable additional experience (including unpublished work in our group), namely, SECKART-ICL. The keyword SECKART ("single Eckart") denotes the procedure in which a single Eckart potential is fit to the differences between the higher level and lower level energies.[10] The keyword DECKART ("dual Eckart") denotes the procedure in which the dual-level energies are the sum of the values from the lower level and the difference of two Eckart functional fits to two individual data point sets from the lower and the higher level method.[11] The keyword ICA indicates that the dual-level frequencies are corrected based on the arithmetic difference of the frequencies.[10] The keyword ICL means that the frequencies are corrected based on the logarithm of the ratio.[11]

2.4. VTST-IOE. In present work, we also introduce another method to perform the dual-level calculations. In this case, the interpolation scheme is the same as the VTST-IOC algorithm explained in the previous section, except that the harmonic analysis is not carried at the higher level. Therefore, both the energy and moments of inertia are corrected as indicated in the VTST-IOC method, but the frequencies along the reaction path are not corrected. We called this method VTST-IOE to denote VTST with interpolated optimized energies.

2.5. Electronic Structure Methods. The following treatments of electron exchange and correlation will be employed:

HF, Hartree–Fock;[19] MP2, Møller–Plesset second-order perturbation theory;[19,30] QCISD(T), quadratic configuration interaction based on single and double excitations and perturbative inclusion of connected triple excitations;[31] BLYP, DFT based on the Becke gradient functional[32] for exchange and the Lee–Yang–Parr (LYP) functional[33] for correlation; B3PW91, Becke's three-parameter hybrid HF-DFT[21] based on the PW91 gradient functional[34] for correlation; B3P86, Becke's three-parameter hybrid HF-DFT approach but based on Perdew's 1986 gradient functional[35] for correlation; B3LYP, Becke's three-parameter hybrid HF-DFT approach but based on the LYP functional for correlation;[22] AM1, Austin model 1;[36] AM1-SRP Austin model 1 with specific reaction parameters[7a,37] adjusted for reaction R3.[10] These treatments are combined with the following basis sets: STO-3G,[38] 3-21G,[39] 6-31G,[40] 6-31G*,[40] 6-311G**,[41] and cc-pVTZ.[42] The AM1 and AM1-SRP models use a minimum basis set.[36]

2.6. Analytic Potential Surface. For reaction R1, we present some calculations using the analytic potential energy function J1 presented previously.[43] This surface was fit in part to experimental data.

2.7. Notation. We denote the Born–Oppenheimer energy of reaction as ΔE and the Born–Oppenheimer barrier height at an optimized saddle point as $V^{\ddagger}$, in both cases exclusive of zero-point energy. In dual-level methods, we denote a barrier height calculated using lower level geometries as $V(s = 0)$, again exclusive of zero-point energy. We denote the imaginary frequency at the saddle point as $\omega^{\ddagger}$, and we denote distance between atoms A and B at the saddle point as $r^{\ddagger}$(AB).

3. Results and Discussion

To test the ISPE procedure, we calculated reaction rates for three atom-transfer reactions,

$$CH_3 + H'H \rightarrow CH_3H' + H \qquad (R1)$$

$$OH + H'H \rightarrow HOH' + H \qquad (R2)$$

$$OH + H'CH_3 \rightarrow HOH' + CH_3 \qquad (R3)$$

with a variety of levels and combinations of levels. All three reactions were treated as bimolecular reactions without recognizing wells, and the vibrational frequencies were evaluated in redundant internal coordinates. For each pair of levels selected for testing dual-level methods, we carried out four types of calculations: (i) single-level calculations at the lower level and higher level; (ii) VTST-IOC calculations by the SECKART-ICA, DECKART-ICL, and SECKART-ICL algorithms (iii) VTST-IOE calculations with energy corrections based on SECKART algorithm; and (iv) VTST-ISPE-$n(l)$ calculations with $n = 0$, 2, 4, and 18. For $n = 2$, we consider nine possible

TABLE 1: Energies, Imaginary Frequency, and Interatomic Distances of Reaction R1

method	ΔE (kcal/mol)	$V^{\ddagger}$ (kcal/mol)	$\omega^{\ddagger}$ (cm^{-1})	$r^{\ddagger}$(CH′) (Å)	$r^{\ddagger}$(H′H) (Å)
J1	−2.77	10.23	988 i	1.346	0.900
HF/STO-3G	0.67	24.47	2738 i	1.302	0.915
MP2/3-21G	−8.30	15.19	1960 i	1.401	0.895
HF/6-31G*	−4.76	20.49	2241 i	1.378	0.923
MP2/6-31G*	−11.23	14.77	1856 i	1.423	0.879
BLYP/6-31G*	−2.47	5.81	962 i	1.448	0.891
B3P86/6-31G*	−3.87	6.00	1046 i	1.433	0.881
B3PW91/6-31G*	−4.91	7.25	1091 i	1.437	0.881
B3LYP/6-31G*	−3.06	7.37	1145 i	1.423	0.890
QCISD(T)/cc-pVTZ	−2.90	12.20		1.395	0.898
MP2/3-21G//J1	−8.54	15.09[a]			
MP2/3-21G//HF/STO-3G	−9.04	13.89[a]			
MP2/6-31G*//BLYP/6-31G*	−11.26	14.77[a]			
MP2/6-31G*//B3P86/6-31G*	−11.25	14.76[a]			
MP2/6-31G*//B3LYP/6-31G*	−11.24	14.77[a]			

[a] $V(s = 0)$.

lists of two s values. The $n = 4$ calculations use two of these pairs, and the $n = 18$ calculations use all nine.

The goal of the present paper is to test systematic methodologies and develop recommendations for the best strategies, *not* to calculate accurate rate constants. Thus, we consider it more useful to test dual-level strategies for cases where the lower and higher levels differ significantly than to test the highest affordable levels. Cases where the lower and higher levels differ significantly provide the biggest challenges to our algorithms for interpolating corrections to the lower level based on a minimum amount of higher level information.

In all cases, we take the single-level calculation at the higher level as the goal of the interpolation method. We ask how close can we come to a full calculation at the higher level if we can afford only a limited number of higher-level calculations, either geometry optimizations, energies, and Hessian at reactants, saddle point, and products for VTST-IOC calculations or single-point energies at $n + 3$ geometries for VTST-ISPE calculations.

To compare the dual-level results with the higher level values, we compute the mean unsigned difference in the logarithm of the calculated rate constant at five temperatures and at four different dynamical levels

$$\mathrm{MUDL} = \frac{1}{20}\sum_{i=1}^{5}\sum_{j=1}^{4}|\log_{10} k^{j}_{\mathrm{X}}(T_i) - \log_{10} k^{j}_{\mathrm{HL}}(T_i)| \quad (14)$$

where T_i is one of five temperatures (300, 400, 600, 1000, and 1500 K), j is one of the four dynamical methods (TST, CVT, CVT/ZCT, CVT/SCT), HL denotes the higher level, and X denotes the lower-level (LL), the VTST-IOC (///) result, the VTST-IOE, or the VTST-ISPE (//) result.

For most of the calculations, we set the scaling mass μ^{25} equal to 1.0 amu, the exception being the calculations with J1 as the lower level where we used $\mu = 1.78$ amu. (Calculated rate constants are independent of μ, but step sizes and potential curves do depend on μ.) All calculations were performed on an SGI Origin 2000 supercomputer.

3.1. Reaction R1. Table 1 gives a survey of the energy of reaction and saddle-point properties calculated for reaction R1 with a variety of electronic structure levels and also with the J1 potential energy surface. The most reliable results are J1 and QCISD(T)/cc-pVTZ. The combinations we selected as best for testing the theory are MP2/3-21G as "higher level" with the J1 or HF/STO-3G as "lower level" and MP2/6-31G* as "higher level" with BLYP/6-31G*, B3PW86, or B3LYP as "lower level".

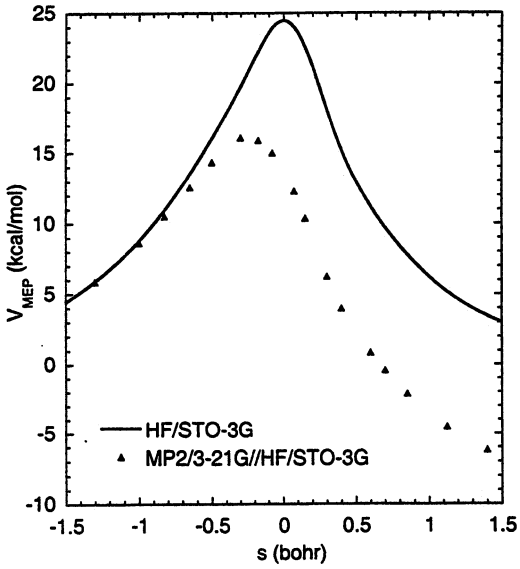

Figure 1. The Born−Oppenheimer energy along the reaction path for R1 calculated at the HF/STO-3G level is shown as a solid curve, and the solid triangles are single-point energy calculations at the MP2/3-21G//HF/STO-3G level. The reduced mass is 1 amu.

The calculations with MP2/3-21G as the higher level provide a very challenging test of theory because, as seen in Table 1, ΔE as calculated at the lower level deviates from the higher level by 6−9 kcal/mol, $V^{\ddagger}$ is off by −5 to +9 kcal/mol, $\omega^{\ddagger}$ is off by ~800−1000 cm^{-1}, and $r^{\ddagger}$(CH′) is off by 0.055−0.10 Å. Table 1 also shows the single-point energy calculations at the lower level saddle-point geometry, which remove a large part of the error in the lower level barrier height. We remind the reader that errors in this paper are always measured with respect to full calculations at the "higher level" involved in the test and are not errors with respect to experiment.

Figure 1 shows what happens when MP2/3-21G single-point calculations are carried out along the HF/STO-3G reaction path. Since HF/STO-3G predicts a positive ΔE, a late transition state is expected according to Hammond's postulate,[44] and Table 1 shows that this indeed is what we found. As a consequence, Figure 1 shows that the maximum of the potential energy profile at the MP2/3-21G//HF/STO-3G level is shifted toward reactants compared to the HF/STO-3G reaction path.

The maximum of the higher level $V_{\mathrm{RP}}(s)$ along the lower level path is 15.09 kcal/mol for MP2/3-21G//J1, which is in reasonable agreement with the full high-level result of 15.19 kcal/mol in Table 1.

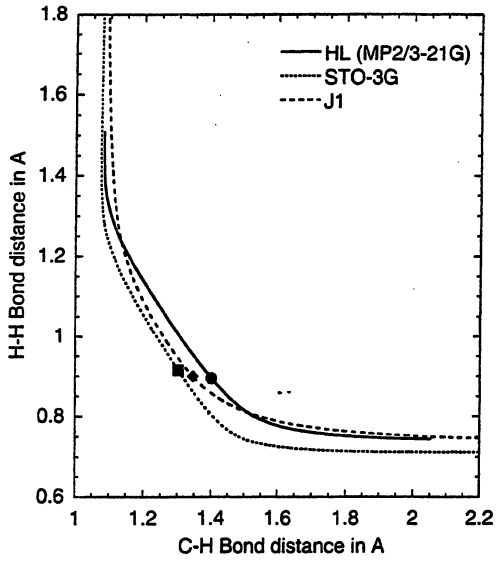

Figure 2. Bond lengths of the H−H and C−H bonds of reaction R1 in angstroms. The solid curve represents the MP2/3-21G calculation with the saddle point indicated as a solid circle, the dotted line is the HF/STO-3G single-level calculation with the saddle point as a solid square, and the dashed line is the calculation based on the analytical potential energy surface J1 with the saddle point as a solid diamond.

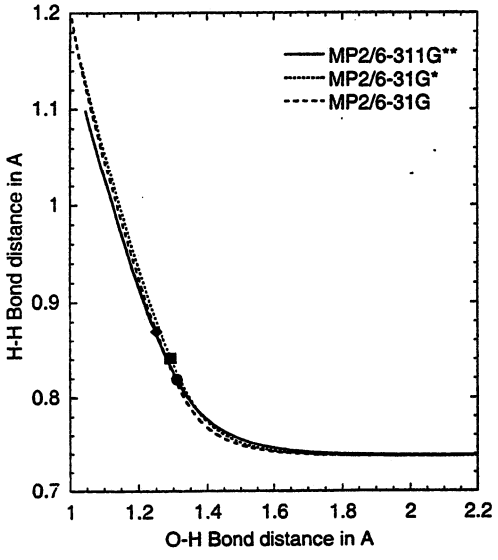

Figure 3. Bond lengths in angstroms of the H−H and C−H bonds along the reaction path of reaction R1. The MP2/6-31G* calculation is shown as a solid line with the saddle point as a solid circle. The BLYP/6-31G* calculation is indicated as a dotted line with the saddle point as a solid square. The B3LPY/6-31G* calculation is indicated as a short-dashed line with the saddle point as a solid diamond, and the B2LYP/6-31G* calculation is indicated as a long dashed line with the saddle point as a solid triangle.

The single-point energies obtained by the MP2/6-31G* higher level with DFT and hybrid HF-DFT methods as the lower level are also tabulated in Table 1. The results are typical in that DFT and hybrid HF-DFT methods underestimate the barrier height, which is the usual case. Since the geometries of the stationary points at the lower level are close to the higher level ones in this case, the interpolated position of the saddle point at the dual level is not shifted far from the saddle point optimized at the lower level (i.e., not shifted far from $s = 0$). Figures 2 and 3 illustrate how the reaction paths agree better for the MP2/6-31G* tests than for the MP2/3-21G tests. Thus, we anticipate that the MP2/3-21G tests will provide a greater challenge for interpolation methods for calculating rate constants.

TABLE 2: Mean Unsigned Difference in Logarithm of the Rate Constant for Reaction R1 at the X///Y or X//Y Level

X =	MP2/3-21G		MP2/6-31G*		
Y =	J1	HF/STO-3G	BLYP	B3LYP	B3P86
lower level	1.90	3.51	3.47	2.83	3.35
IOC-SECKART-ICA	0.21	0.28	0.04	0.02	0.01
IOC-DECKART-ICL	0.43	0.35	0.29	0.29	0.28
IOC-SECKART-ICL	0.21	0.29	0.04	0.02	0.02
IOE-SECKART	0.27	0.29	0.09	0.06	0.05
ISPE-0	0.22	0.34	0.11	0.10	0.09
ISPE-2 (±0.1)	0.38	0.31	0.11	0.06	0.06
ISPE-2 (±0.2)	0.28	0.63	0.11	0.06	0.06
ISPE-2 (±0.4)	0.19	0.89	0.12	0.07	0.07
ISPE-2 (±0.6)	0.15	0.85	0.13	0.07	0.07
ISPE-2 (±0.8)	0.12	0.96	0.13	0.07	0.07
ISPE-2 (±1.0)	0.11	0.90	0.13	0.07	0.07
ISPE-2 (±1.2)	0.20	0.86	0.14	0.07	0.07
ISPE-2 (±1.6)	0.18	0.62	0.15	0.08	0.07
ISPE-2 (±2.0)	0.25	0.68	0.18	0.09	0.08
ISPE-4 (±0.8, ±0.1)	0.12	0.83	0.13	0.08	0.07
ISPE-4 (±0.8, ±0.2)	0.12	0.82	0.13	0.08	0.07
ISPE-4 (±0.8, ±0.4)	0.13	0.91	0.13	0.08	0.07
ISPE-4 (±1.0, ±0.1)	0.10	0.64	0.14	0.08	0.07
ISPE-4 (±1.0, ±0.2)	0.11	0.86	0.14	0.08	0.07
ISPE-4 (±1.0, ±0.4)	0.12	0.91	0.14	0.08	0.07
ISPE-4 (±1.0, ±0.6)	0.11	0.78	0.14	0.08	0.07
ISPE-4 (±1.0, ±0.8)	0.11	0.69	0.14	0.08	0.07
ISPE-4 (±1.0, ±1.2)	0.12	0.68	0.14	0.08	0.07
ISPE-4 (±1.0, ±1.6)	0.15	0.75	0.15	0.08	0.08
ISPE-4 (±1.0, ±2.0)	0.16	0.83	0.16	0.09	0.09
ISPE-4 (±1.2, ±0.1)	0.12	0.55	0.14	0.09	0.08
ISPE-4 (±1.2, ±0.2)	0.12	0.87	0.14	0.09	0.07
ISPE-4 (±1.2, ±0.4)	0.12	0.92	0.14	0.09	0.07
ISPE-4 (±1.6, ±0.1)	0.17	0.52	0.16	0.10	0.08
ISPE-4 (±1.6, ±0.2)	0.17	0.86	0.16	0.10	0.08
ISPE-4 (±1.6, ±0.4)	0.16	0.92	0.16	0.10	0.08
ISPE-4 (±1.6, ±0.8)	0.16	0.76	0.15	0.09	0.08
ISPE-18	0.13	0.93	0.16	0.10	0.08

The dynamics calculations with J1 as the lower surface were carried out with a modified version of Polyrate7.9.1[47] with the higher level information obtained from calculations with Gaussian94.[46] The other calculations were carried with a modified version of Gaussrate7.9.1.[48] The reaction paths were followed using the Page−McIver algorithm,[45] with a step size of $0.001a_0$, except for the B3LYP/6-31G* calculation, which used a step size of $0.005a_0$ to avoid numerical instability. The Hessians were evaluated at every 25 gradient steps for three of the cases, with the exceptions being every five steps for the J1 and every two steps for the B3LYP/6-31G* calculations. The small-curvature tunneling calculation is performed with 40 coordinate points for each action integral and Boltzmann averaged using 40 energies (but only 10 energies for J1). All calculations assign the symmetry number of the forward reaction as 2. Vibrational frequencies were evaluated based on a set of redundant internal coordinates[13c,27] that consists of five stretches, six bends, and one doubly degenerate linear bend.

The tests of the rate constant methods are shown in Table 2. This table can be used to make two kinds of comparisons: (1) compare the MUDL of different dual-level methods; (2) compare the MUDL of the VTST-ISPE method with different numbers of extra points used for spline fits. The VTST-IOC method with SECKART for the energy correction and the ICA scheme for the frequency corrections is shown to be the best dual-level method in overall performance. However, the VTST-IOC option with DECKART for the energy correction and the

TABLE 3: Energies, Imaginary Frequency, and Interatomic Distances of Reaction R2

level	ΔE (kcal/mol)	$V^{\ddagger}$ (kcal/mol)	$\omega^{\ddagger}$ (cm^{-1})	$r^{\ddagger}$(OH') (Å)	$r^{\ddagger}$(H'H) (Å)
MP2/6-31G	−9.73	15.88	2509 i	1.252	0.870
MP2/6-31G*	−18.77	12.87	2229 i	1.292	0.842
MP2/6-311G**	−19.21	9.85	1725 i	1.311	0.819
MP2/6-311G**//MP2/6-31G	−18.37	9.59[a]			
MP2/6-311G**//MP2/6-31G*	−19.10	9.92[a]			

[a] V (s = 0).

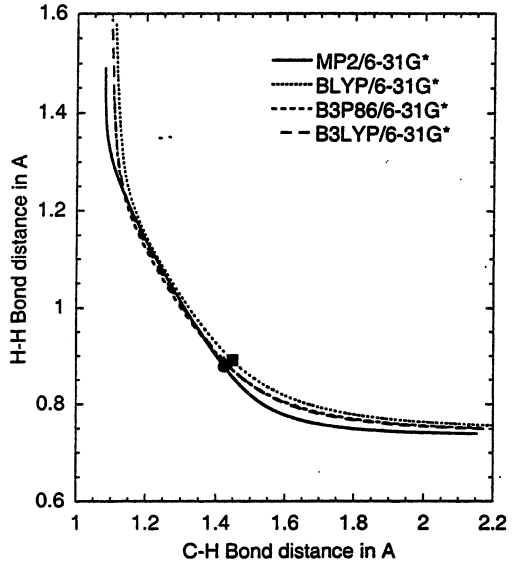

Figure 4. Bond lengths in angstroms of the H−H and C−H bonds along the reaction path of reaction R2. The MP2/6-311G** calculation is shown as a solid line with the saddle point as a solid circle. The MP2/6-31G* calculation is shown as a dotted line with the saddle point as a solid square. And the MP2/6-31G calculation is shown as a dashed line with the saddle point as a solid diamond.

ICL scheme for the frequency corrections is the worst dual-level correction method because it gives a barrier width that is too narrow. Therefore, we only use the SECKART option for the energy correction in the VTST-IOE calculations. The results from the calculations using the VTST-IOE method are expected to be worse than those from the VTST-IOC method because the rate constants obtained from the conventional transition state theory in the VTST-IOC method are exactly the same as the single higher level calculation, but they are different in the VTST-IOE method.

The VTST-ISPE-0 method gives intermediate results. One might think that the result should become better if we keep adding more and more single-point energies for the spline fit. However, the VTST-ISPE calculations with 18 extra points are not systematically better than ISPE-0. The best case is to use four nonstationary points along the low-level reaction path, where two points are close to the 300 K turning points and are useful primarily to estimate the width of the barrier and two other points are close to the lower level saddle point and are useful primarily to locate the dual-level saddle point. (As indicated earlier, the dual-level saddle point is no longer at s = 0.)

3.2. Reaction R2. Table 3 shows the energy, frequency, and geometry information for reaction R2, and Figure 4 shows the reaction path at different levels. The MP2/6-31G calculation predicts a longer breaking-bond distance than does the higher level MP2/6-311G** calculation by about 0.05 Å; however, the saddle-point geometry obtained from the MP2/6-31G* calculation differs from the higher level calculation by only 0.03 Å. The MP2/6-31G calculation predicts a later transition state than does the MP2/6-31G** calculation.

TABLE 4: Mean Unsigned Difference in Logarithm of the Rate Constant for Reaction R2 at the X///Y or X//Y Level

X =	MP2/6-311G**	
Y =	MP2/6-31G	MP2/6-31G*
lower level	2.17	1.06
IOC-SECKART-ICA	0.05	0.02
IOC-DECKART-ICL	0.10	0.11
IOC-SECKART-ICL	0.07	0.09
IOE-SECKART	0.14	0.08
ISPE-0	0.22	0.07
ISPE-2 (±0.1)	0.41	0.10
ISPE-2 (±0.2)	0.40	0.11
ISPE-2 (±0.4)	0.42	0.13
ISPE-2 (±0.6)	0.46	0.17
ISPE-2 (±0.8)	0.50	0.20
ISPE-2 (±1.0)	0.55	0.18
ISPE-2 (±1.2)	0.59	0.18
ISPE-2 (±1.6)	0.64	0.18
ISPE-2 (±2.0)	0.68	0.19
ISPE-4 (±0.8, ±0.1)	0.45	0.13
ISPE-4 (±0.8, ±0.2)	0.43	0.13
ISPE-4 (±0.8, ±0.4)	0.42	0.12
ISPE-4 (±1.0, ±0.1)	0.47	0.14
ISPE-4 (±1.0, ±0.2)	0.44	0.13
ISPE-4 (±1.0, ±0.4)	0.42	0.13
ISPE-4 (±1.0, ±0.6)	0.43	0.13
ISPE-4 (±1.0, ±0.8)	0.46	0.12
ISPE-4 (±1.0, ±1.2)	0.47	0.14
ISPE-4 (±1.0, ±1.6)	0.47	0.16
ISPE-4 (±1.0, ±2.0)	0.48	0.16
ISPE-4 (±1.2, ±0.1)	0.49	0.14
ISPE-4 (±1.2, ±0.2)	0.44	0.13
ISPE-4 (±1.2, ±0.4)	0.42	0.13
ISPE-4 (±1.6, ±0.1)	0.51	0.14
ISPE-4 (±1.6, ±0.2)	0.44	0.13
ISPE-4 (±1.6, ±0.4)	0.42	0.12
ISPE-4 (±1.6, ±0.8)	0.45	0.13
ISPE-18	0.42	0.13

The single-level reaction paths were calculated with the Page−McIver algorithm[45] with a step size of $0.001a_0$, and the Hessians were evaluated at every 20th gradient step. The vibrational frequencies were evaluated with nonredundant internal coordinates.[27] (Since R2 has a chainlike transition state, $3N - 6$ internal coordinates are enough to describe the generalized transition states.) The electronic energy, gradients and Hessians were obtained with the electronic structure package Gaussian94,[46] and the dynamics calculations were carried out with a modified version of Gaussrate7.9.1.[48] The small-curvature tunneling calculation was performed with 40 coordinate points for each action integral and Boltzmann averaged using 40 energies. For both R2 and R3, the partition function includes both the $^2\Pi_{3/2}$ and $^2\Pi_{1/2}$ states of OH. The symmetry number of reaction R2 is 2.

Table 4 shows the MUDL values from calculations with single-level and dual-level methods. Since the MP2/6-31G saddle point and reaction path differ from the MP2/6-311G** one more than the MP2/6-31G* path does or much more than the deviation for any of the three cases in Table 2, we expect a larger MUDL value for MP2/6-311G*//MP2/6-31G in Table

TABLE 5: Energies, Imaginary Frequency, and Interatomic Distances of Reaction R3

level	ΔE (kcal/mol)	$V^{\ddagger}$ (kcal/mol)	$\omega^{\ddagger}$ (cm^{-1})	$r^{\ddagger}$(OH') (Å)	$r^{\ddagger}$(CH') (Å)
AM1	−21.15	11.12	1729 i	1.352	1.204
AM1-SRP	−13.28	7.37	1445 i	1.367	1.211
AM1-SRP//AM1	−11.34	7.37[a]			

[a] V ($s = 0$).

4, and indeed that is what we observe. The VTST-IOC scheme provides reaction rates much closer to the true high-level calculation than does the VTST-ISPE procedure. The ISPE-0 scheme works better than adding more nonstationary points for the interpolation.

3.3. Reaction R3. Table 5 shows energetic information for reaction R3. The specific reaction parameters (SRP) are taken from the previous work[10] where only the oxygen atom parameters were modified in order to obtain better agreement with more reliable values for the classical barrier height (7.4 kcal/mol) and the exoergicity (13.3 kcal/mol). The AM1 method predicts a much higher barrier and lower exoergicity than the more reliable AM1-SRP surface.

The energies for both the AM1 and AM1-SRP models were obtained from the Mopac, version 5.07mn, computer program.[49] The dynamics calculations were carried out with a modified version of the Morate7.9.1 program.[50] The reaction path is followed using the Page−McIver algorithm[45] with the cubic algorithm to estimate the first step from the saddle point. The gradient is calculated every $0.002a_0$, and the Hessian is evaluated at every $0.01a_0$. The vibrational frequencies are evaluated based on a set of 18 redundant internal coordinates,[13c,27] which consists of seven stretches, eight bends, and three torsions. The lowest real harmonic frequency, which is related to the hindered rotation between the OH and CH_3, is very small or imaginary along the reaction path, so a hindered rotation approximation would be appropriate for comparison to experiment, but only the harmonic approximation is applied in the present work. The numerical step size used for the Hessian evaluation is $0.012a_0$. The small-curvature tunneling calculation was performed with 30 coordinate points for each action integral and Boltzmann averaged using 30 energies. The symmetry number of the reaction is 12.

Table 6 tabulates the MUDL values of R3 when AM1, AM1-SRP///AM1, and AM1-SRP//AM1 are compared to AM1-SRP. We see that using the combination of SECKART and ICL for the VTST-IOC procedure provides the best dual-level results. Adding more nonstationary points for the spline interpolation in the VTST-ISPE procedure improves the reaction rate and therefore generates a smaller MUDL value. Having four nonstationary points that are close to the turning points at the 300 K SCT representative energy results in a MUDL value as small as the SECKART-ICL combination.

3.4. Comprehensive Overview. The eight cases in Tables 2, 4, and 6 provide a variety of cases that allow us to search for a robust, best-compromise method that does as well as possible on all of them. Table 7 therefore presents MUDL values averaged over all eight cases. Since each individual MUDL already represented 20 tests of the methods (four dynamical levels and five temperatures), the results in Table 7 represent an average over 160 test cases. Since methods that do well for one or another reaction do not necessarily do well in other cases, all our final conclusions are based in Table 8.

First, consider the IOC methods. As far as average errors are concerned, the original SECKART scheme works better than the newer DECKART scheme, and we now retract our 1997 recommendation to use the latter. The choice between ICA and ICL options has less effect on the average errors. Although the ICA option gives a slightly smaller error, we recommend the ICL option because it has an important qualitative advantage, namely, it never predicts unphysical negative frequencies.[11]

Next, consider the VTST-ISPE results. First of all, we see that using a dense set of points, e.g., VTST-ISPE-18, has no advantage over using only two or four nonstationary points or even zero nonstationary points. Nevertheless, there are two test cases, the first case in Table 2 and the case in Table 6, where $n > 0$ gives significantly better results than $n = 0$, and one might be tempted to try $n > 0$. If one does so, Table 8 shows that putting the first two points very close to the saddle point is the best strategy. Having made this choice, the best location for adding two more points appears to be close to the turning

TABLE 6: Mean Unsigned Difference in Logarithm of the Rate Constant for Reaction R3 at the AM1-SRP///AM1 or AM1-SRP//AM1 Level

procedure	MUDL
lower level	1.27
IOC-SECKART-ICA	0.13
IOC-DECKART-ICL	0.21
IOC-SECKART-ICL	0.07
IOE-SECKART	0.07
ISPE-0	0.35
ISPE-2 (±0.1)	0.12
ISPE-2 (±0.2)	0.12
ISPE-2 (±0.4)	0.10
ISPE-2 (±0.6)	0.08
ISPE-2 (±0.8)	0.09
ISPE-2 (±1.0)	0.10
ISPE-2 (±1.2)	0.13
ISPE-2 (±1.6)	0.15
ISPE-2 (±2.0)	0.31
ISPE-4 (±0.8, ±0.1)	0.12
ISPE-4 (±0.8, ±0.2)	0.12
ISPE-4 (±0.8, ±0.4)	0.11
ISPE-4 (±1.0, ±0.1)	0.12
ISPE-4 (±1.0, ±0.2)	0.12
ISPE-4 (±1.0, ±0.4)	0.11
ISPE-4 (±1.0, ±0.6)	0.10
ISPE-4 (±1.0, ±0.8)	0.08
ISPE-4 (±1.0, ±1.2)	0.08
ISPE-4 (±1.0, ±1.6)	0.09
ISPE-4 (±1.0, ±2.0)	0.15
ISPE-4 (±1.2, ±0.1)	0.13
ISPE-4 (±1.2, ±0.2)	0.13
ISPE-4 (±1.2, ±0.4)	0.11
ISPE-4 (±1.6, ±0.1)	0.14
ISPE-4 (±1.6, ±0.2)	0.14
ISPE-4 (±1.6, ±0.4)	0.12
ISPE-4 (±1.6, ±0.8)	0.09
ISPE-18	0.12

TABLE 7: Mean Unsigned Difference in Logarithm as a Function of Temperature

	300 K	400 K	600 K	1000 K	1500 K
lower level	4.183	3.286	2.290	1.446	1.011
IOC-SECKART-ICL	0.235	0.147	0.066	0.040	0.035
IOE-SECKART	0.248	0.145	0.075	0.079	0.105
ISPE-0	0.312	0.212	0.142	0.133	0.134
ISPE-2 (±0.1)	0.313	0.232	0.159	0.127	0.136
ISPE-4 (±0.1, ±1.2)	0.310	0.256	0.191	0.162	0.157

TABLE 8: Average Mean Unsigned Difference in Logarithm of 160 Calculated Rate Constants

procedure	average MUDL
lower level	2.444
IOC-SECKART-ICA	0.095
IOC-DECKART-ICL	0.256
IOC-SECKART-ICL	0.100
IOE-SECKART	0.131
ISPE-0	0.187
ISPE-2 (±0.1)	0.194
ISPE-2 (±0.2)	0.223
ISPE-2 (±0.4)	0.246
ISPE-2 (±0.6)	0.245
ISPE-2 (±0.8)	0.265
ISPE-2 (±1.0)	0.263
ISPE-2 (±1.2)	0.278
ISPE-2 (±1.6)	0.258
ISPE-2 (±2.0)	0.306
ISPE-4 (±0.8, ±0.1)	0.242
ISPE-4 (±0.8, ±0.2)	0.237
ISPE-4 (±0.8, ±0.4)	0.247
ISPE-4 (±1.0, ±0.1)	0.221
ISPE-4 (±1.0, ±0.2)	0.244
ISPE-4 (±1.0, ±0.4)	0.247
ISPE-4 (±1.0, ±0.6)	0.230
ISPE-4 (±1.0, ±0.8)	0.219
ISPE-4 (±1.0, ±1.2)	0.223
ISPE-4 (±1.0, ±1.6)	0.241
ISPE-4 (±1.0, ±2.0)	0.263
ISPE-4 (±1.2, ±0.1)	0.217
ISPE-4 (±1.2, ±0.2)	0.248
ISPE-4 (±1.2, ±0.4)	0.251
ISPE-4 (±1.6, ±0.1)	0.227
ISPE-4 (±1.6, ±0.2)	0.259
ISPE-4 (±1.6, ±0.4)	0.260
ISPE-4 (±1.6, ±0.8)	0.239
ISPE-18	0.259

points for the tunneling calculation at the representative tunneling energy for the lowest temperature of interest, i.e., VTST-ISPE (±0.1, ±1.0) or VTST-ISPE (±0.1, ±1.2). The major conclusion though is the counterintuitive one that, if one employs our mapped interpolation, there is no systematic advantage in adding single-point energies all along the reaction path or even calculating any higher level single-point energies at nonstationary points. This conclusion is not entirely a negative result. It leads to the following positive recommendation. Instead of dividing one resources over $n + 3$ or $n + 4$ single-point energies, one should use only three or four points and use the resulting savings to raise the level of electronic structure theory.

Notice that using the uncorrected lower level gives a MUDL of 2.444 or typical error of $10^{2.444}$, which is a factor of 278. The best ISPE strategy, ISPE-0, reduces the typical error to $10^{0.187}$, which is a factor of 1.54. The IOC-SECKART-ICL method further reduces the typical error to a factor of $10^{0.100}$, which is a factor of 1.26. Thus, the VTST-IC approach is very powerful and the recommendations for optimum VTST-IOC and VTST-ISPE strategies should be very useful.

Why does it not pay to keep adding more points in the VTST-ISPE method? If the higher level reaction path differs from the lower level one, then the single-point higher level calculations along the lower level reaction path are not being calculated along the higher level valley floor but rather part way up the valley walls of the higher level valley.[17a] This means that if one searches for the maximum higher level energy along the lower level path, the result will be systematically too high. That is why we originally recommended using geometry optimization at the higher level.[10] The popularity of the single-point energy approach, though, caused us to develop and evaluate this method systematically. It is very pleasing that our mapped interpolation scheme lets one recover essentially the full advantage of single-point energy corrections from a very small set of such corrections, namely corrections only at the stationary points.

In light of the above explanation, we believe that our conclusions concerning the VTST-ISPE methodology are not dependent on the particular interpolating scheme that we have used.

Having evaluated the methods over a range of temperatures, it is interesting to consider the MUDL values of the final most highly recommended strategies as functions of temperature. Each entry in Table 7 is an average of 32 cases (four dynamical levels and eight combinations of higher and lower electronic structure levels). In Table 7, we see that the MUDL decreases as the temperature increases. Thus, the dominant error contribution comes from the lower temperatures. This is because the tunneling effect is important at the low temperature, and tunneling depends on the barrier width, which is harder to correct than the barrier height.

In Table 9, we compare the bond lengths of the making and breaking bonds at distances -1.2α and $1.2\alpha'$ from the lower level saddle point. As described above, the values of α and α' are determined based on the turning points for SCT representative tunneling energies at 300 K. This table shows that the tunneling region over which the potential representation should be refined is typically a few tenths of an angstrom in width.

In Table 10, we compare the highest energy point obtained from the interpolation based on the single-point calculations along the lower level reaction path to the corrected energy at $s = 0$ and to the true barrier height obtained from the higher level at the optimized saddle-point geometry. The max $V^{HL/LL}(s)$ value is calculated based on a parabolic fit to the three highest energy single-point calculations from a set of 19 points (18 nonstationary points plus $s = 0$). We observe that the max $V^{HL/LL}(s)$ value is greater than the energy of the higher level saddle point $V^{\ddagger,HL}$ for all cases. This will always be the case because the minimum energy path (MEP) at the lower level is different from the higher level one. There is no advantage, on the average, in following the procedure (that has been recommended by other workers) of finding the maximum of $V^{HL/LL}(s)$ over the reaction path as compared to just evaluating $V^{HL/LL}(s)$ at the lower level saddle point.

TABLE 9: Bond Lengths of Making and Breaking Bonds in A + HB → AH + B at Critical Points along Reaction Path

		$s = -1.2\|\alpha\|$		$s = 1.2\alpha'$	
reaction	level	r(A−H) (Å)	r(H−B) (Å)	r(A−H) (Å)	r(H−B) (Å)
R1	J1	1.610	0.786	1.211	1.070
	HF/STO-3G	1.760	0.715	1.462	1.075
	BLYP/6-31G*	1.706	0.793	1.375	0.949
	B3LYP/6-31G*	1.705	0.780	1.316	0.990
	B3P86/6-31G*	1.647	0.793	1.354	0.947
R2	MP2/6-31G	1.767	0.738	1.065	1.096
	MP2/6-31G*	1.787	0.738	1.143	1.003
R3	AM1	1.726	1.109	1.215	1.325

TABLE 10: Comparison of the Energy of Highest Energy Point along Lower Level Path to the Value at $s = 0$ and to the Energy at the Geometry Optimized at the Higher Level (V^{HL})

higher level	lower level	$V^{\ddagger,HL}$	$V^{HL/LL}(s=0)$	$\max V^{HL/LL}(s)$
MP2/3-21G	J1	15.19	15.09	15.52
	HF/STO-3G	15.19	13.89	16.17
MP2/6-31G*	BLYP/6-31G*	14.77	14.77	14.80
	B3LYP/6-31G*	14.77	14.77	14.76
	B3P86/6-31G*	14.77	14.76	14.77
MP2/6-311G**	MP2/6-31G	9.85	9.59	10.17
	MP2/6-31G*	9.85	9.92	9.96
AM1-SRP	AM1	7.37	7.37	7.40
average |deviation| from $V^{\ddagger,HL}$			0.22	0.23

TABLE 11: Mean Unsigned Difference in Logarithm at Different Dynamical Levels

	TST	CVT	CVT/ZCT	CVT/SCT
lower level	2.654	2.628	2.362	2.130
IOC-SECKART-ICL	0.000	0.053	0.145	0.201
IOE-SECKART	0.094	0.101	0.136	0.190
ISPE-0	0.206	0.164	0.171	0.206
ISPE-2 (±0.1)	0.173	0.207	0.197	0.197
ISPE-4 (±0.1, ±1.2)	0.173	0.225	0.241	0.222

In the VTST-IOC scheme, interpolations are based on information about the reactants, products, and saddle point (or reactant well, product well, and saddle point) at the higher level; the corrected barrier is used at the $s = 0$ position based on a true geometry-optimized barrier height obtained from the higher level. However, with the VTST-ISPE scheme, the maximum of $V^{HL/LL}$ points is generally shifted in the s direction and is larger than the true barrier height. Therefore, VTST-ISPE calculations (or similar schemes that correct energies based on the reaction path from a lower level) are less reliable than VTST-IOC. The present paper adds to evidence previously[10,11] that the VTST-IOC method provides a good approximation to reaction rate constants.

Next, we return to Table 7 and consider the IOE algorithm. Table 7 shows that this is only slightly less accurate than IOC at temperatures up to 600 K. The main advantage of improving the frequencies is that it yields much more accurate results at T = 1000 K. The fact that the IOE results are uniformly better than the ISPE ones shows the overriding importance of optimizing the saddle-point geometry at the highest possible level.

Table 11 is like Table 7, except that the results are sorted by dynamical level rather then temperature. Ultimately, for practical applications, one is mainly interested in the accuracy for the highest dynamical level, CVT/SCT. But, we decided to include all four dynamical levels in our evaluation of the quality of the methods because the other levels are useful for interpretive purposes and because they show whether one is getting the correct answers at the highest level for the right reason or because of cancellation of errors. The IOC-SECKART-ICL scheme does best on average across all four levels, whereas the ISPE schemes do worst. However, all the interpolated correction methods are much better than using the uncorrected low-level results at any of the four levels of dynamics.

Although we have not given any X//X'///Y results in this paper, the results do have implications for that kind of approach. In particular, they show the importance of carrying out the X' step at as high a level as possible.

4. Conclusion

The VTST-ISPE method allows one to correct potential energies along a reaction path with only a few single-point calculations. The present paper presents a mapped interpolation scheme for recovering essentially the full benefit of higher level single-point energy corrections on the basis of carrying out such calculations only at the stationary points, which should provide useful computer resource savings for future applications. Although the VTST-ISPE is successful at reducing the errors, the VTST-IOC method results in much more accurate rate constants on the average for three different reactions with eight different pairs of higher and lower levels. Because the lower level reaction path deviates from the minimum energy path that would be obtained with the higher level of electronic structure theory, applying single-point energy corrections based on the lower level geometries results in too large a value for the corrected barrier height. Therefore, we recommend VTST-IOC as a more reliable dual-level method for reaction rate calculations based on the direct dynamics scheme when geometry optimization at the higher level is computationaly affordable. It is also possible to perform the VTST-IOC calculation without the corrections in frequencies, and we denote this method as VTST-IOE. The results from the VTST-IOE calculations are significantly worse than the VTST-IOC results at high temperatures. Nevertheless, they are still more accurate than VTST-ISPE calculations over the whole temperature range. The VTST-IOE method shows us the value of carrying out a higher level geometry optimization procedure in the dual-level schemes. It is better to carry out more accurate calculations including geometry optimization at the three stationary points than to carry out many additional single-point energy calculations along the whole reaction path.

Acknowledgment. This work was supported in part by the U.S. Department of Energy, Office of Basic Energy Sciences. J.C.C. acknowledges the Spanish Ministerio de Educación y Cultura and the Fulbright Commission for a postdoctoral scholarship.

References and Notes

(1) (a) Truhlar, D. G.; Garrett, B. C. *Annu. Rev. Phys. Chem.* **1984**, *35*, 159. (b) Allison, T. C.; Truhlar, D. G. In *Modern Methods for Multidimensional dynamics Computations in Chemistry*; Thompson, D. L., Ed.; World Scientific: Singapore, 1998; p 618−712.

(2) Truhlar, D. G.; Garrett, B. C.; Klippenstein, S. J. *J. Phys. Chem.* **1996**, *100*, 12771.

(3) (a) Wonchoba, S. E.; Hu, W.-P.; Truhlar, D. G. In *Theoretical and Computational Approaches to Interface Phenomena*; Sellers, H. L., Golab, J. T., Eds.; Plenum: New York, 1994. (b) Garrett, B. C.; Schenter, G. K. *Int. Rev. Phys. Chem.* **1994**, *13*, 263. (c) Chuang, Y.-Y.; Cramer, C. J.; Truhlar, D. G. *Int. J. Quantum Chem.* **1998**, *70*, 887.

(4) (a) Doubleday, C., Jr.; McIver, J. W., Jr.; Page, M. *J. Phys. Chem.* **1988**, *92*, 4367. (b) Baldridge, K. K.; Gordon, M. S.; Steckler, R.; Truhlar, D. G. *J. Phys. Chem.* **1989**, *93*, 5107.

(5) Garrett, B. C.; Koszykowski, M. L.; Melius, C. F.; Page, M. *J. Phys. Chem.* **1990**, *94*, 7096.

(6) Truhlar, D. G.; Gordon, M. S. *Science* **1990**, *249*, 491.

(7) (a) Gonzalez-Lafont, A.; Truong, T. N.; Truhlar, D. G. *J. Phys. Chem.* **1991**, *95*, 4618. (b) Storer, J. W.; Houk, K. N. *J. Am. Chem. Soc.* **1993**, *115*, 10426.

(8) Liu, Y.-P.; Lu, D.-h.; Gonzalez-Lafont, A.; Truhlar, D. G.; Garrett, B. C. *J. Am. Chem. Soc.* **1993**, *115*, 7806.

(9) Truhlar, D. G. In *The Reaction Path in Chemistry*; Heidrich, D., Ed.; Kluwer: Dordrecht, 1995; p 229.

(10) Hu, W.-P.; Liu, Y.-P.; Truhlar, D. G. *J. Chem. Soc., Faraday Trans.* **1994**, *90*, 1715.

(11) Chuang, Y.-Y.; Truhlar, D. G. *J. Phys. Chem.* A **1997**, *101*, 3808; **1997**, *101*, 8741.

(12) (a) Marcus, R. A. *Discuss. Faraday Soc.* **1967**, *44*, 167. (b) Shavitt, I. *J. Chem. Phys.* **1968**, *49*, 4048. (c) Truhlar, D. G.; Kuppermann, A. *J. Am. Chem. Soc.* **1971**, *93*, 1840. (d) Garrett, B. C.; Truhlar, D. G. *J. Chem. Phys.* **1979**, *70*, 1593. (e) Skodje, R. T.; Truhlar, D. G.; Garrett, B. C. *J. Phys. Chem.* **1981**, *85*, 3019.

(13) (a) Miller, W. H.; Handy, N. C.; Adams, J. E. *J. Chem. Phys.* **1980**, *72*, 99. (b) Corchado, J. C.; Espinosa-Garcia, J.; Hu, W.-P.; Rossi, I.; Truhlar, D. G. *J. Phys. Chem.* **1995**, *99*, 687. (c) Chuang, Y.-Y.; Truhlar, D. G. *J. Phys. Chem. A* **1998**, *102*, 242.

(14) (a) Morokuma, K.; Kato, S. In *Potential Energy Surfaces and Dynamics Calculations*; Truhlar, D. G., Ed.; Plenum: New York, 1981; pp 243–264. (b) Colwell, S. M.; Handy, N. C. *J. Chem. Phys.* **1985**, *82*, 1281.

(15) (a) Garrett, B. C.; Truhlar, D. G.; Wagner, A. F.; Dunning, T. H., Jr. *J. Chem. Phys.* **1983**, *78*, 4400. (b) Bondi, D. K.; Connor, J. N. L.; Garrett, B. C.; Truhlar, D. G. *J. Chem. Phys.* **1983**, *78*, 5981.

(16) Page, M. *Comput. Phys. Comm.* **1994**, *84*, 115.

(17) (a) Espinosa-García, J.; Corchado, J. C. *J. Phys. Chem.* **1995**, *99*, 8613. (b) Truong, T. N.; Duncan, W. T.; Bell, R. L. *ACS Symp. Ser.* **1996**, *629*, 85.

(18) (a) Petersson, G. A. *ACS Symp. Ser.* **1998**, *677*, 237. (b) Malick, D. K.; Petersson, G. A.; Montgomery, J. A., Jr. *J. Chem. Phys.* **1998**, *108*, 5704.

(19) Hehre, W. J.; Radom, L.; Schleyer, P. v. R.; Pople, J. A. *Ab Initio Molecular Orbital Theory*: John Wiley & Sons: New York, 1986.

(20) Ziegler, T. *Chem. Rev.* **1991**, *91*, 651.

(21) Becke, A. D. *J. Chem. Phys.* **1993**, *98*, 1372.

(22) Stephens, P. J.; Devlin, F. J.; Ashvar, C. S.; Bak, K. L.; Taylor, P. R.; Frisch, M. J. *ACS Symp. Ser.* **1996**, *629*, 105.

(23) Glasstone, S.; Laidler, K. J.; Eyring, H. *Theory of Rate Processes*; McGraw-Hill: New York, 1941.

(24) Garrett, B. C.; Truhlar, D. G. *J. Chem. Phys.* **1979**, *70*, 1593.

(25) (a) Garrett, B. C.; Truhlar, D. G.; Grev, R. S.; Magnuson, A. W. *J. Phys. Chem.* **1980**, *84*, 1730; **1983**, *87*, 4554(E). (b) Truhlar, D. G.; Isaacson, A. D.; Skodje, R. T.; Garrett, B. C. *J. Phys. Chem.* **1982**, *86*, 2261; **1983**, *87*, 4554(E). (c) Truhlar, D. G.; Isaacson, A. D.; Garrett, B. C. In *Theory of Chemical Reaction Dynamics*; Baer, M., Ed.; CRC Press: Boca Raton, 1985; Vol. 4, p 65.

(26) Liu, Y.-P.; Lynch, G. C.; Truong, T. N.; Lu, D.-h; Truhlar, D. G.; Garrett, B. C. *J. Am. Chem. Soc.* **1993**, *115*, 2408.

(27) (a) Jackels, C. F.; Gu, Z.; Truhlar, D. G. *J. Chem. Phys.* **1995**, *102*, 3188. (b) Nguyen, K. A.; Jackels, C. F.; Truhlar, D. G. *J. Chem. Phys.* **1996**, *104*, 6491. (c) Chuang, Y.-Y.; Truhlar D. G. *J. Chem. Phys.* **1997**, *107*, 83.

(28) (a) Renka, R. J. SIAM *J. Stat. Comput.* **1987**, *8*, 393. (b) Renka, R. J. *ACM Trans. Math. Software* **1993**, *19*, 81.

(29) Corchado, J. C.; Coitiño, E. L.; Chuang, Y.-Y.; Fast, P. L.; Truhlar, D. G. *J. Phys. Chem. A* **1998**, *102*, 2424.

(30) Møller, C.; Plesset, M. S. *Phys. Rev.* **1934**, *46*, 618.

(31) Pople, J. A.; Head-Gordon, M.; Raghavachari, K. *J. Chem. Phys.* **1987**, *87*, 5968.

(32) Becke, A. D. *Phys. Rev. A* **1988**, *38*, 3098.

(33) Lee, C.; Yang, W.; Parr, R. G. *Phys. Rev. B* **1988**, *37*, 785.

(34) (a) Perdew, J. P. In *Electronic Structure of Solids '91*; Ziesche, P., Eschrig, H., Eds.; Akademie Verlag: Berlin, 1991; p 11. (b) Perdew, J. P.; Chevary, J. A.; Vosko, S. H.; Jackson, K. A.; Pederson, M. R.; Singh, D. J.; Foilhaus, C. *Phys. Rev. B* **1992**, *46*, 6671. (c) Perdew, J. P.; Burke, K.; Ernzerhof, M. *ACS Symp. Ser.* **1996**, *629*, 453. (d) Perdew, J. P.; Burke, K.; Wang, Y. *Phys. Rev. B* **1996**, *54*, 16533.

(35) Perdew, J. P. *Phys. Rev. B* **1986**, *33*, 8822.

(36) Dewar, M. J. S.; Zoebisch, E. G.; Heely, E. F.; Stewart, J. J. P. *J. Am. Chem. Soc.* **1985**, *107*, 3902.

(37) Liu, Y.-P.; Lu, D.-h; Gonzalez-Lafont, A.; Truhlar, D. G.; Garrett, B. C. *J. Am. Chem. Soc.* **1993**, *115*, 7806.

(38) (a) Binkley, J. S.; Pople, J. A.; Hehre, W. J. *J. Am. Chem. Soc.* **1980**, *102*, 939. (b) Gordon, M. S.; Binkley, J. S.; Pople, J. A.; Pietro, W. J.; Hehre, W. J. *J. Am. Chem. Soc.* **1982**, *104*, 2797.

(39) (a) Hehre, W. J.; Stewart, R. F.; Pople, J. A. *J. Chem. Phys.* **1969**, *51*, 2657. (b) Collins, J. B.; Schleyer, P. v. R.; Binkley, J. S.; Pople, J. A. *J. Chem. Phys.* **1976**, *64*, 5142.

(40) (a) Ditchfield, R.; Hehre, W. J.; Pople, J. A. *J. Chem. Phys.* **1971**, *54*, 724. (b) Hehre, W. J.; Ditchfield, R.; Pople, J. A. *J. Chem. Phys.* **1972**, *56*, 2257.

(41) (a) McLean, A. D.; Chandler, G. S. *J. Chem. Phys.* **1980**, *72*, 5639. (b) Krishnan, R.; Binkley, J. S.; Seeger, R.; Pople, J. A. *J. Chem. Phys.* **1980**, *72*, 650.

(42) Dunning, T. H. *J. Chem. Phys.* **1989**, *90*, 1007.

(43) (a) Steckler, R.; Dykema, K. J.; Brown, F. B.; Hancock, G. C.; Truhlar, D. G.; Valencich, T. *J. Chem. Phys.* **1987**, *87*, 7024. (b) Joseph, T.; Steckler, R.; Truhlar, D. G. *J. Chem. Phys.* **1987**, *87*, 7630.

(44) (a) Hammond, G. S. *J. Am. Chem. Soc.* **1955**, *77*, 334. (b) Parr, C. A.; Truhlar, D. G. *J. Phys. Chem.* **1971**, *75*, 1844.

(45) Page, M.; McIver, J. W., Jr. *J. Chem. Phys.* **1988**, *88*, 922.

(46) Frisch, M. J.; Trucks, G. W.; Schlegel, H. B.; Gill, P. M. W.; Johnson, B. G.; Robb, M. A.; Cheeseman, J. R.; Keith, T.; Petersson, G. A.; Montgomery, J. A.; Raghavachari, K.; Al-Laham, M. A.; Zakrzewski, V. G.; Ortiz, J. V.; Foresman, J. B.; Cioslowski, J.; Stefanov, B. B.; Nanayakkara, A.; Challacombe, M.; Peng, C. Y.; Ayala, P. Y.; Chen, W.; Wong, M. W.; Andres, J. L.; Replogle, E. S.; Gomperts, R.; Martin, R. L.; Fox, D. J.; Binkley, J. S.; Defrees, D. J.; Baker, J.; Stewart, J. J. P.; Head-Gordon, M.; Gonzalez, C.; Pople, J. A. *Gaussian94*; Gaussian, Inc.: Pittsburgh, PA, 1995.

(47) Corchado, J. C.; Chuang, Y.-Y.; Fast, P. L.; Villà, J.; Coitiño, E. L.; Hu, W.-P.; Liu, Y.-P.; Lynch, G. C.; Nguyen, K.; Jackels, C. F.; Gu, M. Z.; Rossi, I.; Clayton, S.; Melissas, V.; Steckler, R.; Garrett, B. C.; Isaacson, A. D.; Truhlar, D. G. *Polyrate7.9.1*; University of Minnesota, 1998 [http://comp.chem.umn.edu/polyrate].

(48) Corchado, J.; Coitiño, E. L.; Chuang, Y.-Y.; Truhlar, D. G. *Gaussrate7.9.1*; University of Minnesota, 1998 (based on *polyrate7.9.1*[47] and *Gaussian94*[46] [http://comp.chem.umn.edu/gaussrate]).

(49) Stewart, J. J. P.; Rossi, I.; Hu, W.-P.; Lynch, G. C.; Liu, Y.-P.; Truhlar, D. G. *Mopac*, version 5.07mn; University of Minnesota, 1997 [http://comp.chem.umn.edu/mopac].

(50) Chuang, Y.-Y.; Fast, P. L.; Hu, W.-P.; Lynch, G. C.; Liu, Y.-P.; Truhlar, D. G. *Morate7.9.1*; University of Minnesota, 1998 (based on *polyrate7.9.1*[47] and *Mopac*, version 5.07mn[49] [http://comp.chem.umn.edu/morate].